01 Jun 2022

Synthesis Of Dysprosium Oxychloride (DyOCl)

Saehwa Chong

Brian J. Riley

José Marcial

Charmayne E. Lonergan
Missouri University of Science and Technology, clonergan@mst.edu

et. al. For a complete list of authors, see https://scholarsmine.mst.edu/matsci_eng_facwork/3216

Recommended Citation

S. Chong et al., "Synthesis Of Dysprosium Oxychloride (DyOCl)," *Journal of Chemical Crystallography*, vol. 52, no. 2, pp. 185 - 193, Springer, Jun 2022.
The definitive version is available at https://doi.org/10.1007/s10870-021-00904-2

Journal of Chemical Crystallography (2022) 52:185–193
https://doi.org/10.1007/s10870-021-00904-2

ORIGINAL PAPER

Synthesis of Dysprosium Oxychloride (DyOCl)

Saehwa Chong[1] · Brian J. Riley[1] · José Marcial[1] · Charmayne E. Lonergan[1] · Derek A. Cutforth[1]

Received: 28 December 2020 / Accepted: 1 September 2021 / Published online: 24 September 2021

Abstract

Dysprosium oxychloride, DyOCl, was synthesized using a simple hydrolysis method with $DyCl_3{\cdot}6H_2O$. X-ray powder diffraction (XRD) data was used to determine the crystal structure. The DyOCl compound is isostructural to the matlockite (PbFCl) crystal structure and crystallizes in the tetragonal *P*4/*nmm* (#129) space group. The crystal structure contains the alternating cationic layers of $(DyO)_n$ and anionic layers of $n{Cl}^-$ along the *c*-axis. The structural data including unit cell, volume, and density of DyOCl were compared to other rare-earth oxychloride data from the Inorganic Crystal Structure Database (ICSD) and our previous study on TbOCl. Fourier-transform infrared spectroscopy was performed on DyOCl and peaks observed at 543 and 744 cm^{-1} were attributed to Dy–O and Dy–Cl. Scanning electron microscopy analysis showed irregularly shaped crystals. Hot-stage XRD, thermogravimetry, as well as differential scanning calorimetry coupled to a gas chromatograph and a mass spectrometer (evolved gas analysis) were performed on $DyCl_3{\cdot}6H_2O$ to understand the phase transformation to DyOCl (and Dy_2O_3) as a function of temperature and time at temperature.

Graphic Abstract

DyOCl compound with the tetragonal P4/nmm space group is composed of the alternating layers of $(DyO)_n$ and $n{Cl}^-$ along the *c*-axis.

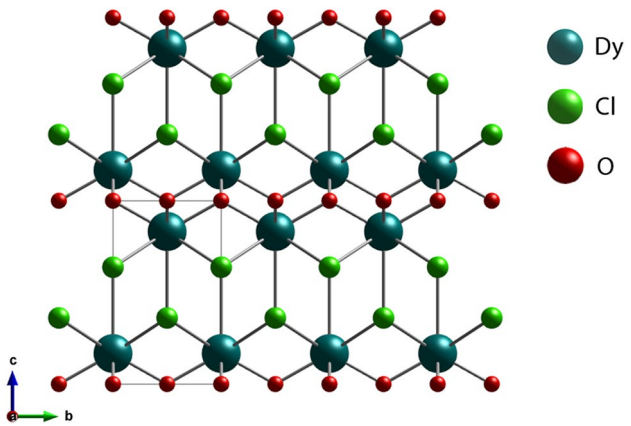

Keywords Oxychloride · Rare-earth elements · Dysprosium

Introduction

Rare-earth oxychlorides (REOCl) are used for a range of applications such as catalysis [1–3], phosphors [4, 5], and sensors [6, 7] due to unique optical and chemical properties attributed to the RE elements. Podkolzin et al. [1] showed that a LaOCl catalyst converted methane to methyl

✉ Saehwa Chong
saehwa.chong@pnnl.gov

[1] Pacific Northwest National Laboratory, Richland, WA 99352, USA

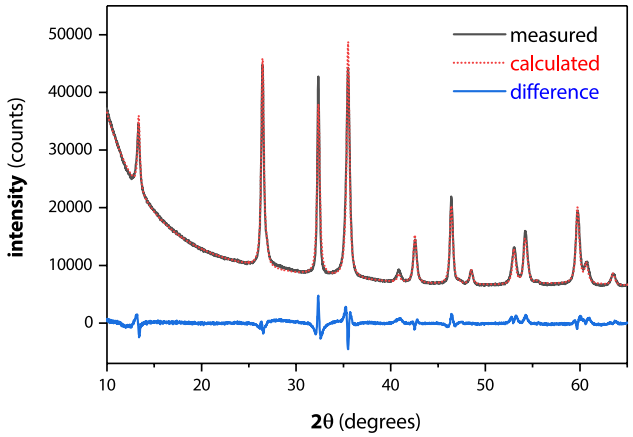

Fig. 1 Measured, calculated, and difference XRD patterns of DyOCl

chloride and was stable for three weeks. Sharfe et al. [3] synthesized a highly efficient EuOCl catalysts for converting ethylene to vinyl chloride. Morassaei et al. [2] synthesized a NdOCl-$Nd_2Sn_2O_7$-SnO_2 nanocomposite with better photocatalytic performance than a SnO_2 nanocrystalline catalyst.

As a phosphor material, Kim et al. [4] synthesized blue-emitting Eu^{2+} activated LaO*X* (*X* = Cl, Br, I) and showed that the emission spectra can be shifted by incorporating different halide anions into the structure, resulting in changes of La–*X* bond lengths and stronger crystal fields for smaller halide anions. Kim et al. [5] later synthesized blue- and red-emitting EuO*X* (*X* = F, Cl, Br, I) crystals and showed that oxidation states of Eu and the vibration modes of the resulting Eu–*X* and Eu–O bonds changed the emitting wavelengths. The EuO*X* compounds with the Eu site occupied by the mixed Eu^{2+} and Eu^{3+} cations resulted in a blue-emitting compound whereas, when the Eu site was fully occupied by Eu^{3+}, this resulted in a red-emitting compound.

For sensor applications, Marsal et al. [6] investigated a nanocrystalline LaOCl compound to detect CO_2 gas using diffuse reflectance infrared Fourier transform spectroscopy (DRIFTS). Imanaka et al. [7] synthesized the Ca-doped LaOCl electrode with Cl^- ion vacancies to detect Cl_2 gas. With Mg^{2+} and O^{2-} ion conductors, the Ca-doped LaOCl electrode showed fast responses to detect Cl_2 gas with high stability even at elevated temperatures of 980 ℃ [7].

In addition, REOCl compounds are useful for remediation of RE fission products. During pyrochemical reprocessing of used nuclear fuel to recover actinides, different salts of $FPCl_x$ are formed where FP denotes fission products of alkali metals, alkaline-earth metals, and REs. The resulting $RECl_3$ compounds can be precipitated from chloride wastes as REOCl and/or REO_x through oxygen sparging or reactive precipitation with carbonates, and then these REOCl/REO_x mixtures can be incorporated into glass waste forms [8]. Glass-based waste forms including lead tellurite, lanthanide borosilicates, and lanthanide aluminoborosilicates can be used to immobilize these RE-based precipitates [9–12].

This paper discusses the simple synthesis method and crystal structure of DyOCl, which was not previously reported in the Inorganic Crystal Structure Database (ICSD). Here, powder X-ray diffraction (P-XRD), Fourier-transform infrared spectroscopy (FTIR), and scanning electron microscopy (SEM) were used to characterize the structural properties of DyOCl. Other in-situ characterization techniques were also employed to assess thermal conversions of $DyCl_3{\cdot}6H_2O$ to DyOCl and Dy_2O_3. The calculated structural parameters for DyOCl including the unit cell parameters, unit cell volume, and density were compared to values of other of REOCl compounds in the literature to understand the trends for these types of compounds and this study fills a gap in RE-series of REOCl compounds in the ICSD.

Experimental

Synthesis

A pure polycrystalline DyOCl compound was synthesized via a heat treatment of 0.4903 g $DyCl_3{\cdot}6H_2O$ (Alfa Aesar, 99.99%) in air, similar to our previous study with $TbCl_3{\cdot}6H_2O$ [13]. Here, 0.5 g of $DyCl_3{\cdot}6H_2O$ was placed in a 20-mL alumina crucible, heated to 400 ℃ at 5 ℃ min^{-1} inside a Thermolyne box furnace, held for 32 h, and then cooled at 1 °C min^{-1}. The $DyCl_3{\cdot}6H_2O$ converts into DyOCl through a hydrolysis reaction as shown below in Reaction (1) where the byproducts of HCl and H_2O are evolved as gases inside the furnace. This reaction was verified with thermogravimetry (TGA), as well as differential scanning calorimetry (DSC) coupled to a gas chromatograph (GC) and a mass spectrometer (MS).

$$DyCl_3 \cdot 6H_2O_{(s)} \rightarrow DyOCl_{(s)} + 2\,HCl_{(\uparrow)} + 5\,H_2O_{(\uparrow)} \quad (1)$$

Characterizations

X-ray diffraction (XRD) data was collected using a Bruker D8 Advance instrument equipped with a Cu tube and a LynxEye™ position-sensitive detector (Bruker AXS Inc.). For powder-XRD data collection, a zero-background quartz sample holder (MTI corporation) with a cavity of 10-mm diameter and 1-mm deep was filled with the fired powder and loaded into the instrument. The scanning parameters were 5° to 70° 2θ with 0.02° 2θ steps and 2-s dwells per step; the X-ray tube was operated at 40 kV and 40 mA.

Table 1 Crystal data, data collection, and structure refinement details

Compound	Dysprosium oxychloride
Chemical formula	DyOCl
CCDC number	2,052,907
*M*r	214
Space group	*P4/nmm*
Temperature (K)	293
a, *c* (Å)	3.91290(10), 6.6296(3)
V (Å^3)	101.501(6)
Z	2
Appearance	Yellow-white
Radiation type	Cu $K\alpha_1$, $K\alpha_2$, λ = 1.540562, 1.544390 Å
Data Collection	
Diffractometer	Bruker D8 Advance
Specimen mounting	Packed powder pellet
Data collection mode	Reflection
Scan method	Step
2θ values (°)	$2\theta_{min} = 5$, $2\theta_{max} = 68.977$, $2\theta_{step} = 0.019$
Refinement	
R factors and goodness of fit	$R_p = 0.02$, $R_{wp} = 0.04$, $R_{exp} = 0.01$, GOF = 3.98
No. of parameters	20

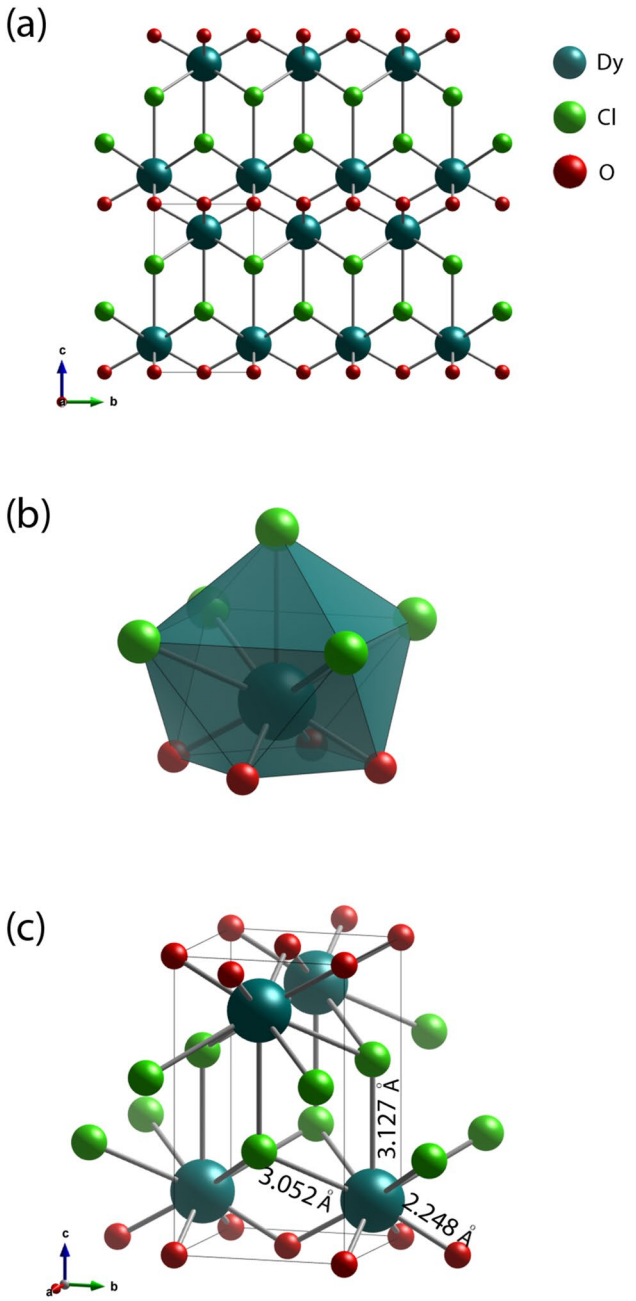

Fig. 2 **a** The crystal structure, **b** the coordination environment of Dy, and **c** the unit cell of the DyOCl compound

For crystal structure determination, the unit cell parameters were obtained using TOPAS (v5) [14] and JANA2006 [15] was used to refine the atomic positions with the obtained unit cell parameters as initial values. The pseudo-Voigt function with other peak-shape parameters were used to fit peaks, and the background was fitted with a Chebychev polynomial. The plot of Rietveld refinement result is shown in Fig. 1. The final refinement converged at $R_{wp} = 3.68\%$.

In-situ hot-stage XRD (HS-XRD) was performed using the Bruker D8 Advance diffractometer using the hot-stage attachment (HTK-16 N, Anton Paar). Then, XRD patterns were collected in three angular ranges including 12°–18° (range-1), 24°–30° (range-2), and 24°–50° 2θ (range-3) with a 0.015° step size and 1.5-s dwells per step. The X-ray beam was confined to a 10-mm irradiated length with a programmable variable divergence slit. Approximately 0.05 g of dry $DyCl_3 \cdot 6H_2O$ powder was placed onto the platinum heater strip and the chamber was closed. An air purge gas was flowed into the sample chamber at a flow rate of 45 mL min^{-1}. For one set of in-situ measurements, sample powder was heated at 5 °C min^{-1} starting from room temperature to 400 °C in 50 °C increments between 50 and 400 °C. During ramp heating from 50 to 350 °C, diffraction patterns were measured over range-1 and range-2. Once the sample reached 400 °C, it was isothermally held and diffraction patterns were measured over range-3. During isothermal heating, the diffraction patterns were first measured every 30 min for 7 h and then every 1 h for 13 h (for a total duration of 33 h). A second HS-XRD run was performed where a new sample of $DyCl_3 \cdot 6H_2O$ powder was placed on the cleaned Pt heater strip, a scan was collected from 24° to 50° 2θ (range-3) with a 0.015° step size and 1.5-s dwells per step, the sample was heated at 10 °C s^{-1} to 400 °C using an air purge gas, and data was collected using the same collection parameters. Data was fit using Rietveld refinements,

Table 2 Structural parameters of REOCl in the ICSD or Cambridge Crystallographic Data Centre (CCDC)* in addition to the DyOCl data from the current study; entry 412069 for CeOCl is a private communication documented in the ICSD from R.L. Harlow, J.M. Novak, and G.P.A. Yap (2004)

RE	a (Å)	c (Å)	V (Å^3)	P (g/cm^3)	ICSD	References
La	4.109	6.865	115.9	5.454	24611	[26]
La	4.117	6.881	116.6	5.420	40297	[21]
La	4.1351	6.9040	118.1	5.355	77815	[24]
La	4.1162	6.8746	116.5	5.428	84330	[25]
Ce	4.0866	6.8538	114.5	5.558	412069	–
Ce	4.0785	6.8346	113.7	5.596	72154	[19]
Pr	4.053	6.799	111.7	5.723	31664	[27]
Nd	4.04	6.77	110.5	5.882	31665	[27]
Nd	4.0249	6.7837	109.9	5.914	59231	[22]
Sm	3.982	6.721	106.6	6.289	26581	[28]
Eu	3.9646	6.6950	105.2	6.420	28529	[29]
Eu	3.9668	6.6955	105.4	6.412	54682	[20]
Gd	3.9495	6.6708	104.1	6.661	59232	[22]
Gd	3.9698	6.7008	105.6	6.564	77820	[24]
Tb	3.9279	6.6556	102.7	6.804	1993793*	[13]
Dy	3.9129	6.6296	101.5	7.000	Current study	
Ho	3.893	6.602	100.1	7.182	76171	[28]

using the software package described above, correcting for the variable divergence slits and sample displacement.

Evolved gas analysis (EGA) was done with a DSC-TGA-GC–MS using a Netzsch 449 F1 Jupiter instrument connected to an Agilent 7890A GC and Agilent 5975 single quadrupole MS. Approximately ~ 20 mg of $DyCl_3{\cdot}6H_2O$ was placed in an alumina crucible and then that was placed onto the DSC sample stage. The sample was held for 20 min at 30 °C before heating at 5 °C min^{-1} to 1000 °C using air as both the purge and protective gas at constant flow rates of 20 mL min^{-1} and 40 mL min^{-1}, respectively. The evolved gases moved from the DSC chamber to the GC–MS using a heated transfer tube and helium as the carrier gas. The gases flowed through the GC sampling loop (250 µL) and were sampled every minute. The GC injector was set to splitless mode. The sampled aliquot was injected into the GC column (GS-CarbonPLOT, 30-m long and 320-µm inner diameter), eluted with He gas, and the species were separated by the column prior to entering the MS for analysis. The GC–MS system measured samples under a He atmosphere with a constant column flow rate of 1.5 mL min^{-1}. The heated system components (e.g., the transfer tubing, sampling loop valve box, and GC column) were set to temperatures greater than 100 °C to reduce potential condensation of gaseous species. The MS ionization energy was set to 20 eV, the scan range *m*/*z* (mass-to-charge ratio) was 10–200, and the GC–MS interface held at 280 °C.

The SEM image was collected with a JSM-7001F field-emission gun microscope (JEOL USA, Inc.; Peabody, MA) using a backscattered electron detector. Prior to analysis, powdered DyOCl was mounted to an aluminium stub using carbon tape and the sample was coated with 2.5 nm of Ir metal using a Quorum 150 T ES (Electron Microscopy Sciences, Hatfield, PA) sputter coater.

The FTIR analysis was performed using a Nicolet 6700 spectrometer (Thermo Fisher Scientific, Waltham, MA). Here, DyOCl was ground to a powder in a Diamonite™ mortar and pestle and mixed with dehydrated KBr (FTIR grade, Alfa Aesar) in a 1:200 mass ratio within the mortar. Then, the mixture was pressed into a pellet using a uniaxial press and a 10-mm diameter steel die. A blank KBr pellet was also made for use as a background. Both pellets were loaded into the transmission cell in the spectrometer and scanned at 64 co-adds with 2 cm^{-1} resolution from 4000 to 400 cm^{-1}. Exported data was plotted in Origin Pro for visualization.

Results and Discussion

Crystal Structure of DyOCl

Crystal data and structure refinement details of the DyOCl compound are summarized in Table 1. The REOCl compounds crystallize within the tetragonal space group of *P4/nmm* (#129) and have matlockite (PbFCl) structures [16]. The crystal structure of DyOCl is composed of alternating (001) layers of (DyO)*n* and *n*Cl$^-$ (Fig. 2a). The Dy^{3+} cations are nine-coordinated by four oxygen ions and five chloride ions, forming a monocapped square antiprism of TbO_4Cl_5 (Fig. 2b). The bond lengths of Dy–Cl are 3.052 Å for the nearest four Cl atoms, 3.127 Å for the apical Cl atom, and the bond length of Dy–O is 2.248 Å (Fig. 2c). The RE–Cl and RE–O distances increase with larger RE cations in the

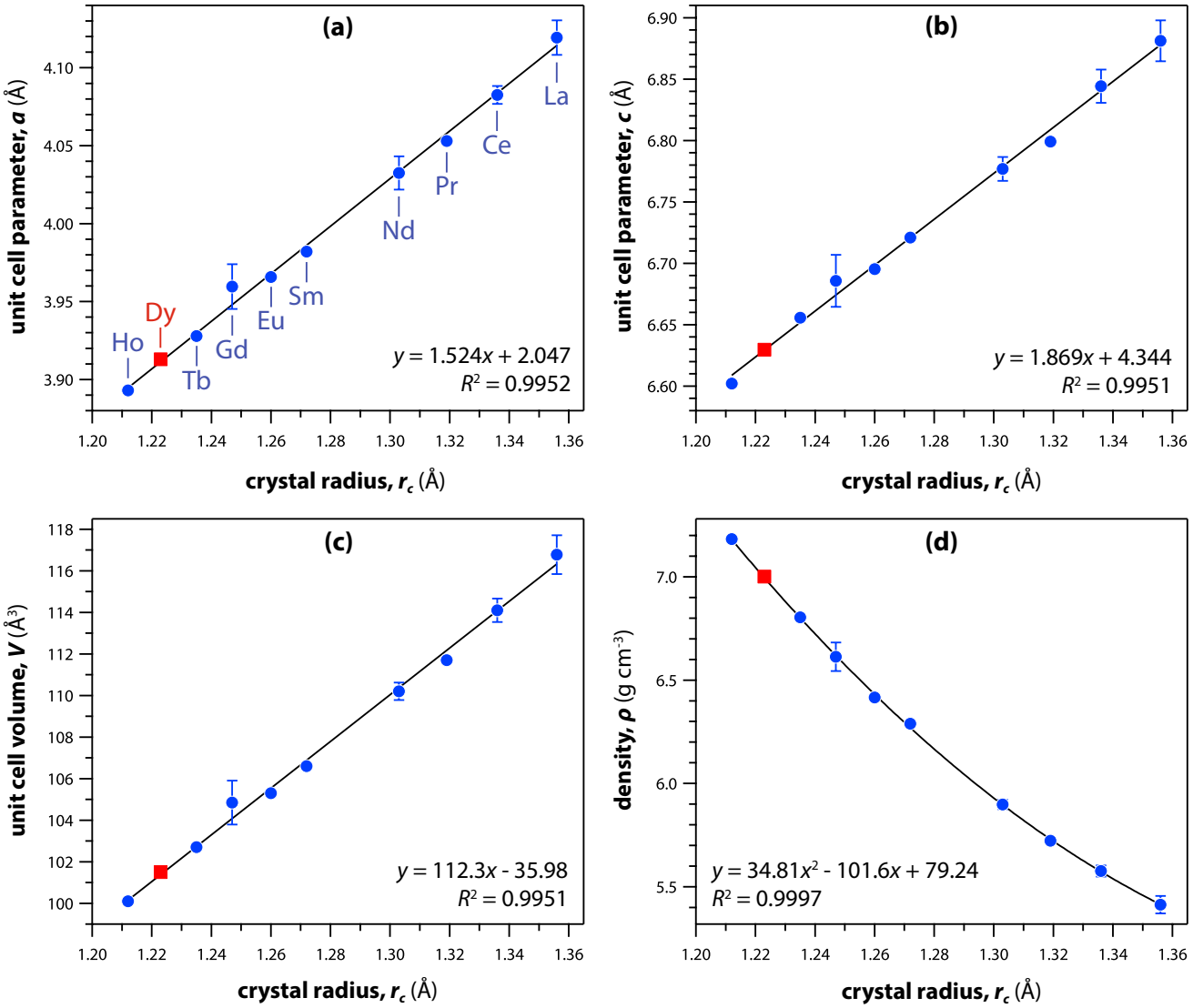

Fig. 3 **a**, **b** Unit cell parameters (*a* and *c*, respectively), **c** unit cell volumes (*V*), and **d** calculated unit cell densities (ρ) of REOCl compounds as a function of the crystal radius of the RE element (coordination = 9) in each according to Shannon (1976) compared to literature values provided in Table 3. The red box in each plot represents DyOCl

structure [13]. Table 2 provides the structural data of REOCl reported in the ICSD or Cambridge Crystallographic Data Centre (CCDC) and from the current study. The structural parameters of DyOCl fit well into the trendline calculated from literature data of REOCl (Fig. 3). With large *RE* cations, the unit cell parameters and volumes increase linearly whereas the densities decrease nonlinearly and fit very well to a 2nd-order polynomial. For multiple data points of the same RE compounds from different literature references, an average value was used for the plots along with standard deviation error bars. The SEM micrograph shows the agglomerate crystallites (Fig. 4), and no clear faceted shapes of crystallites were visible. Figure 5 shows the FTIR spectra of DyOCl with peaks at 534 and 744 cm^{-1} attributed to the stretching of Dy–O and bond vibration of Dy–Cl, respectively [17, 18].

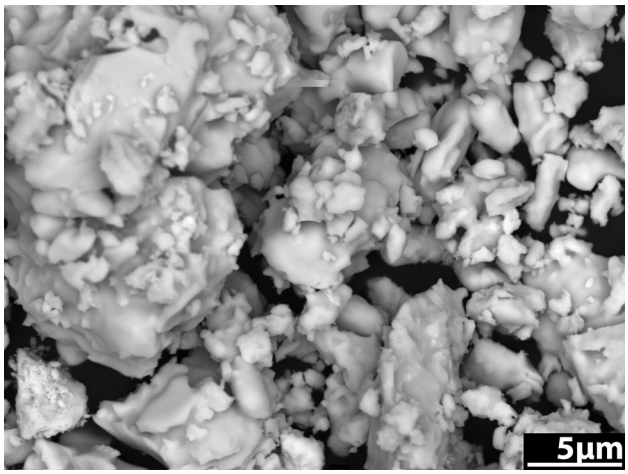

Fig. 4 SEM micrograph of DyOCl compound

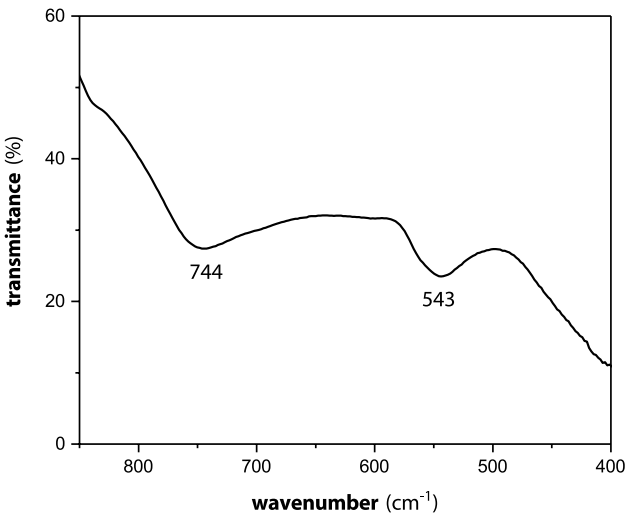

Fig. 5 FTIR spectra of DyOCl compound

Structural Phase Transformation in $DyCl_3 \cdot 6H_2O$

The HS-XRD from the first run is shown in Fig. 6. This data showed that full conversion of $DyCl_3 \cdot 6H_2O$ to DyOCl occurred in the range of 240–400 ℃ (Fig. 6d–f) in less than 2 h. When the temperature reached 400 ℃, the sample was held isothermally, scans were taken in the range of 24°–50° 2θ (Fig. 6c,f), and conversion from DyOCl to Dy_2O_3 was observed after ~ 6 h; full conversion to Dy_2O_3 occurred by 6.94 h (Fig. 6c, f).

This finding was interesting because Dy_2O_3 was not observed during powder XRD where the same reactant was exposed for a similar amount of time at 400 °C. This discrepancy is attributed to a likely temperature offset in the thermocouple (bottom of Pt heater strip) and the sample (top of Pt heater strip). To evaluate the rate of DyOCl conversion with HS-XRD, the second experiment run at 10 °C s^{-1} showed that DyOCl formation was very rapid and on the order of minutes (see Fig. 7).

The results of the EGA on $DyCl_3 \cdot 6H_2O$ showed the evaporation of water in the range of 115 to 185 °C and endothermic peaks at 240 and 350 ℃ are where 2 HCl molecules are evolved from $DyCl_3 \cdot 6H_2O$ to form DyOCl through hydrolysis (Fig. 8)—see Reaction (1). Another endothermic peak around 700 ℃ is due to conversion of DyOCl to Dy_2O_3 through Reaction (2) shown below with moisture present in the DSC furnace.

$$2\,DyOCl_{(s)} + H_2O_{(g)} \rightarrow Dy_2O_{3(s)} + 2\,HCl_{(\uparrow)} \quad (2)$$

Phase transformation from $DyCl_3 \cdot 6H_2O$ to DyOCl occurred rapidly by hydrolysis. Based on the results of the in-situ HS-XRD and EGA, full conversion of $DyCl_3 \cdot 6H_2O$ to DyOCl could be achieved at 350 °C at much shorter times (a few hours at most) than those used in the current study. In addition, DyOCl can be converted to Dy_2O_3 around 400 °C depending on the heating conditions.

Synthesis Methods

Different synthesis methods for REOCl compounds have been used in the literature including solution-based [19], solid-state [19, 20], flux-assisted [16, 21], and metallothermic reduction methods [22] (Table 3), but the hydrolysis method [13] used in the current study is very elegant and simple. The REOCl compounds in the literature are often synthesized as polycrystalline powders, although some single crystals of REOCl have been reported [21, 23]. For the synthesis of polycrystalline REOCl compounds, REO_x with NH_4Cl or $RECl_3 \cdot (H_2O)_x$ precursors are often used [20, 21, 24, 25] whereas chloride fluxes such as $BaCl_2$ or $RECl_3$ are used for syntheses of single crystals [21, 23]. Hölsä et al. [25] annealed a mixture of La_2O_3 and NH_4Cl at 450 °C for 0.5 h, and then heated at 900 °C in a N_2 atmosphere for the synthesis of LaOCl. The cooling rate was not reported, and the resulting product was a pure polycrystalline LaOCl compound [25]. Aitasalo et al. [20] synthesized a pure polycrystalline EuOCl compound using a similar route, in which a mixture of Eu_2O_3 and NH_4Cl was first annealed at 450 °C for 0.5 h and then heated at 750 °C for 1.5 h. Brixner and Moore [21] synthesized polycrystalline LaOCl compounds by heating mixtures of La_2O_3 and NH_4Cl in a 1:1 mass ratio at 300, 500, and 900 °C for 2–4 h each. With these LaOCl powders, single crystals of LaOCl were synthesized using LaOCl powder in $BaCl_2$ flux melted at 1100 °C and cooled to 500 °C at 5 °C h^{-1} [21]. Aride et al. [23] synthesized single crystals of NdOCl using a flux-assisted method, in which

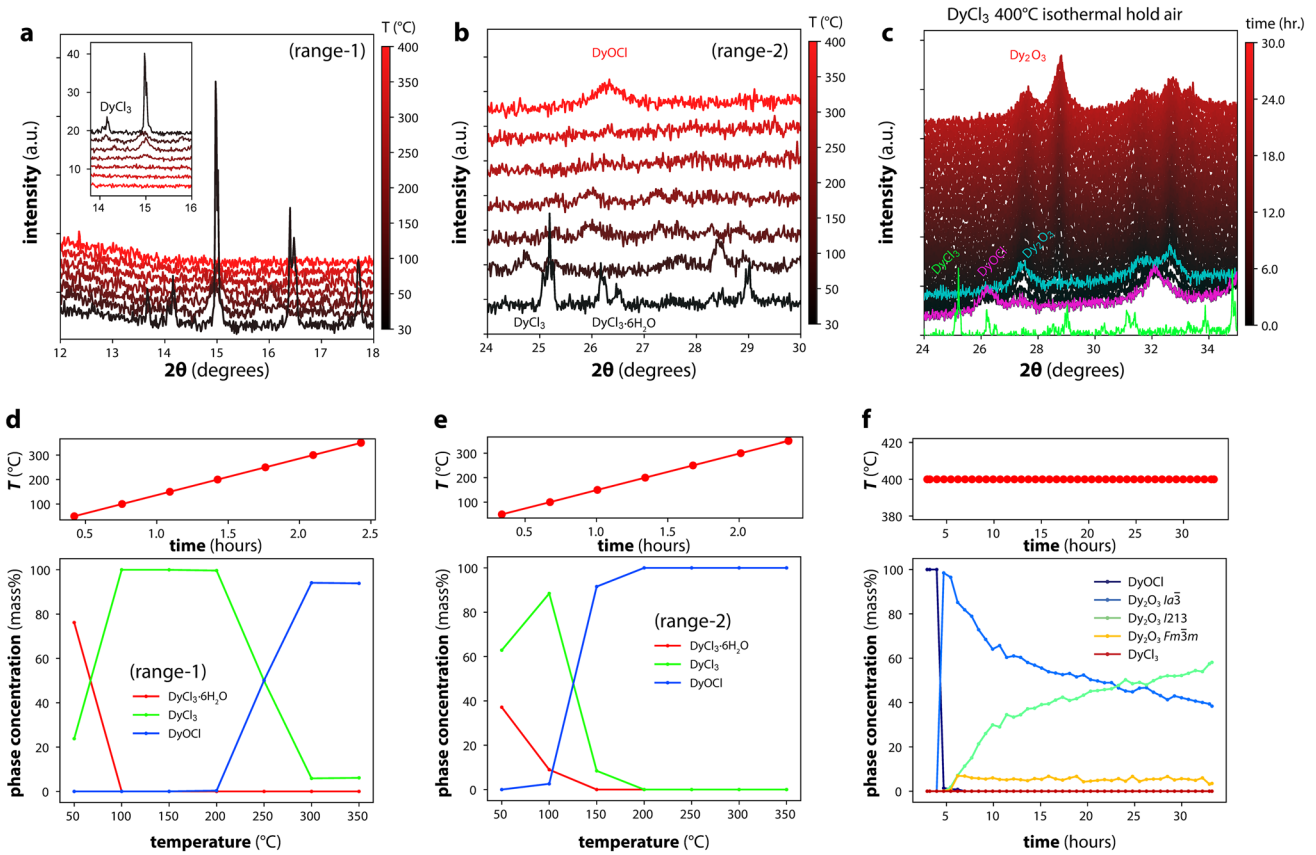

Fig. 6 Summary of HS-XRD run at 5 °C min^{-1} ramp rate showing **a** the change in 12–18° 2θ ($DyCl_3$ peaks) as a function of temperature, **b** the change in 24–30° 2θ ($DyCl_3$, $DyCl_3$-$6H_2O$, and DyOCl peaks) as a function of temperature, **c** a waterfall plot showing the phase transitions as a function of time at 400 °C including a transition to Dy_2O_3, **d** phase concentrations based on quantification using the 12–18° 2θ region, **e** phase concentrations based on quantification using the 24–30° 2θ region, and **f** phase concentrations as a function of time at 400 °C (correlating to **c**)

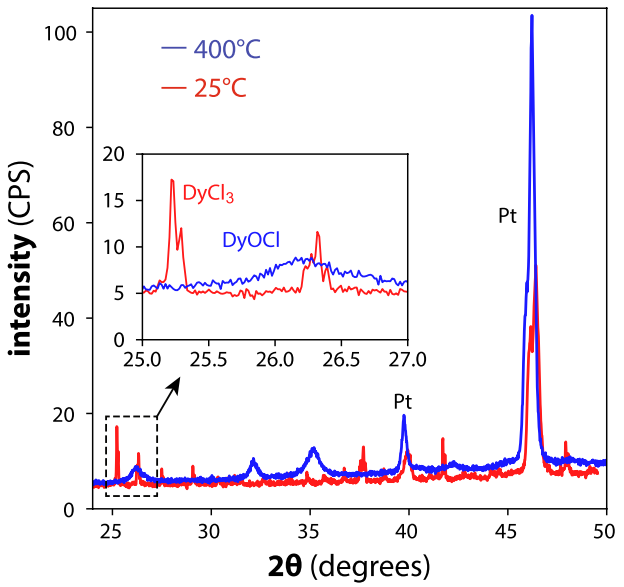

Fig. 7 Diffraction patterns and (inset) magnified region of 25–27° 2θ from HS-XRD run at 10 °C s^{-1} ramp rate showing the before scan (25 °C) and the after scan (400 °C) started ~ 38 s afterwards. For the full 2θ range, the Pt peaks from the heater strip (sample holder) are visible

Nd_2O_3 in $NdCl_3$ flux was heated to 700–900 ℃ for 2–15 h and cooled down to room temperature at 3 °C h^{-1} [23].

These types of crystals have a range of different uses and can be synthesized using a variety of synthesis techniques. While the hydrolysis synthesis approach used in the current study is quite simple to perform, it did not yield REOCl crystals for some of the $RECl_3{\cdot}(H_2O)_x$ precursors evaluated during experiments reported here. In fact, this sample approach was also attempted with $TmCl_3{\cdot}x(H_2O)$, $LuCl_3{\cdot}6H_2O$, and $ErCl_3{\cdot}x(H_2O)$ but these materials formed mixed phases of REOCl and RE_3O_4Cl. It is possible that different heat-treatment conditions could be implemented to achieve the desired REOCl products, but this was not attempted.

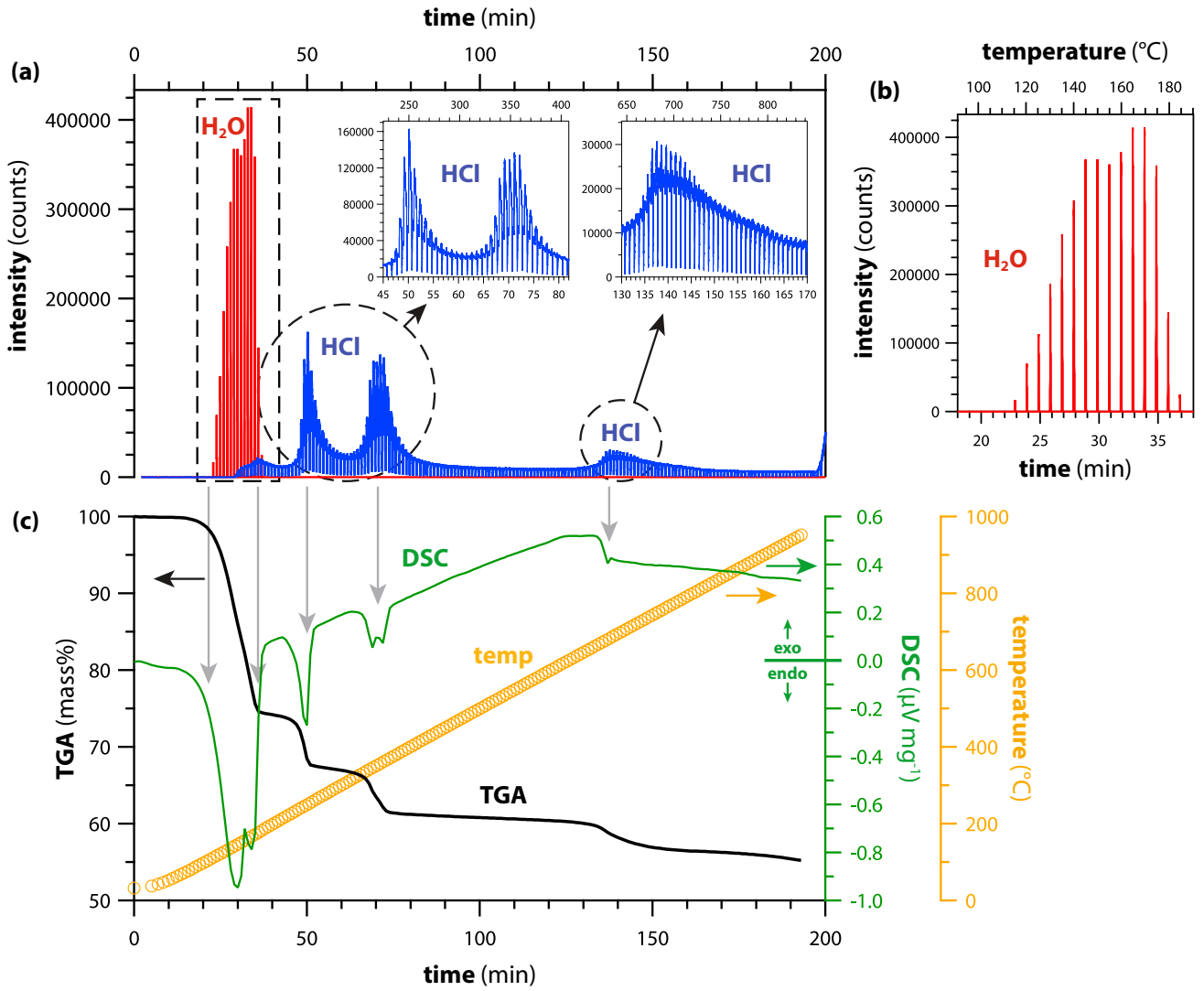

Fig. 8 **a**, **b** GC–MS and **c** TGA–DSC plots of $DyCl_3{\cdot}6H_2O$. For (**a**), the insets are zoomed-in regions of the main plot showing detail for the HCl peaks where the top axes are temperature (°C) and the bottom axes are time (min). For **b**, the same axes are used as the insets in **a** to show the time and temperature range where water was evolving. Offsets in the times between DSC and GC–MS data were calculated (and applied to data) based on the expected delay times through the GC column

Table 3 The synthesis of REOCl with the *P4/nmm* space group in the literature and the current study

RE	Reactants	Synthesis	*T* (℃)	*t* (h)	*r* (℃ h^{-1})	Atm	ICSD	References
La	La_2O_3, NH_4Cl, $BaCl_2$	F	1100	–	5	–	40297	[21]
La	La_2O_3, NH_4Cl	SS	900	–	–	N_2	–	[25]
Ce	CeO_2, $PdCl_2$	SB + SS	627	20	–	H_2	72154	[19]
Nd	$NdCl_3$	MR	850	168	20	Ar_2	59231	[22]
Eu	La_2O_3, NH_4Cl	SS	750	1.5	–	N_2	54682	[20]
Gd	$GdCl_3$	MR	700	240	20	Ar_2	59232	[22]
Tb	$TbCl_3{\cdot}6H_2O$	H	400	8	300	Air	1993793*	[13]
Dy	$DyCl_3{\cdot}6H_2O$	H	400	32	300	Air	Current study	–

H, F, MR, SB, and SS denote hydrolysis, flux-assisted, metallothermic reduction, solution-based, and solid-state syntheses, respectively. Values of T, t, r, and atm denote the maximum reaction temperature, reaction time, cooling rate, and heat-treatment atmosphere used; "*" indicates the Cambridge Crystallographic Data Centre (CCDC) reference number, and—denotes "not provided". ICSD denotes the Inorganic Crystal Structure Database reference number

Conclusions

A pure polycrystalline DyOCl compound was synthesized using a simple hydrolysis method. In-situ HS-XRD and EGA results showed that conversion of $DyCl_3 \cdot 6H_2O$ to DyOCl occurred rapidly by hydrolysis in the temperature range of 250 to 400 ℃ through the evolution of HCl vapor. The structural parameters of DyOCl are in good agreement with other REOCl compounds found in the literature. The unit cell parameters and volumes of REOCl compounds increase linearly with large RE cations in the structures whereas the density decreases nonlinearly according to a 2^{nd}-order polynomial function. The current study fills gaps in the structural data of REOCl in the literature.

Supplementary Information The online version contains supplementary material available at https://doi.org/10.1007/s10870-021-00904-2.

Acknowledgements The Pacific Northwest National Laboratory is operated by Battelle under Contract Number DE-AC05-76RL01830.

References

1. Podkolzin SG, Stangland EE, Jones ME, Peringer E, Lercher JA (2007) J Am Chem Soc 129(9):2569–2576
2. Morassaei MS, Zinatloo-Ajabshir S, Salavati-Niasari M (2016) J Mol Liq 220:902–909
3. Scharfe M, Lira-Parada PA, Amrute AP, Mitchell S, Pérez-Ramírez J (2016) J Catal 344:524–534
4. Kim D, Park S, Kim S, Kang S-G, Park J-C (2014) Inorg Chem 53(22):11966–11973
5. Kim D, Jeong JR, Jang Y, Bae J-S, Chung I, Liang R, Seo D-K, Kim S-J, Park J-C (2019) Phys Chem Chem Phys 21(4):1737–1749
6. Marsal A, Centeno MA, Odriozola JA, Cornet A, Morante JR (2005) Sens Actuators B 108(1–2):484–489
7. Imanaka N, Okamoto K, Adachi G-Y (2001) Electrochem Commun 3(2):49–51
8. Riley BJ (2020) Ind Eng Chem Res 59(21):9760–9774
9. Fadzil SM, Hrma P, Schweiger MJ, Riley BJ (2015) J Nucl Mater 465:657–663
10. Fadzil SM, Hrma P, Schweiger MJ, Riley BJ (2016) J Nucl Mater 478:261–267
11. Riley BJ, Pierce DA, Crum JV, Williams BD, Snyder MMV, Peterson JA (2018) Prog Nucl Energy 104:102–108
12. Riley BJ, Chong S (2020) J Non-Cryst Solids 545:120161
13. Chong S, Riley BJ, Nelson ZJ (2020) Acta Crystallogr. Sect E 76(5):621–624
14. Bruker AXS. *TOPAS, Version 4.2*. 2009.
15. Petrícek V, Dusek M, Palatinus L (2014) Z Kristallogr 229(5):345–352
16. Bannister FA (1934) Mineral Mag J Mineral Soc 23(146):587–597
17. Basile LJ, Ferraro JR, Gronert D (1971) J Inorg Nucl Chem 33(4):1047–1053
18. Wang M, Deng X, Feng J, Yu B, Zhu H, Li X, Zheng X, Bai J, Peng Y (2015) J Alloys Compd 619:681–685
19. Wolcyrz M, Kepinski L (1992) J Solid State Chem 99:409–413
20. Aitasalo T, Hölsä J, Lastusaari M, Legendziewicz J, Lehto L, Lindén J, Maryško M (2004) J Alloys Compd 380(1–2):296–302
21. Brixner LH, Moore EP (1983) Acta Crystallogr Sect C 39(9):1316–1316
22. Meyer G, Schleid T (1986) Z Anorg Allg Chem 533:181–185
23. Aride J, Chaminade J-P, Pouchard M (1982) J Cryst Growth 57(1):194–196
24. Hölsä J, Säilynoja E, Koski K, Rahiala H, Valkonen J (1996) Powder Diffr 11(2):129–133
25. Hölsä J, Lastusaari M, Valkonen J (1997) J Alloys Compd 262:299–304
26. Sillen LG, Nylander AL (1941) Sven Kem Tidskr 53:367–372
27. Zachariasen WH (1949) Acta Crystallogr Sect A 2(6):388–390
28. Templeton DH, Dauben CH (1953) J Am Chem Soc 75(23):6069–6070
29. Bärnighausen H, Brauer G, Schultz N (1965) Z Anorg Allg Chem 338(5–6):250–265